Analytical model of amplitude-weighted array technology in forming symmetrical radiation patterns

Lanxiang Zhong (种兰祥)[1,2], Zhiyong Zhang (张志勇)[1], and Jianlang Li (李建郎)[2*]

[1] *Xi'an Institute of Optics and Precision Mechanics, Chinese Academy of Sciences, Xi'an 710068, China*

[2] *Shanghai Institute of Optics and Fine Mechanics, Chinese Academy of Sciences, Shanghai 201800, China*

[*] *Corresponding author: apuli@siom.ac.cn*

Received March 26, 2013; accepted May 31, 2013; posted online August 2, 2013

A method on amplitude-weighted array technology is proposed based on an analytical formula in which the radiation amplitudes of array elements are evaluated analytically by a random symmetrical far-field radiation pattern. Using this formula, any desired spatial radiation pattern in the far field could be built by applying the analytical solutions of radiation amplitudes of array elements. To check the validity of this formula as well as the proposed technique, an annular intensity distribution as target far-field pattern is designed, and the respective radiation amplitude of array elements are determined by solving the formula analytically. The available far-field pattern is calculated by applying these solutions and then compared with the target far-field pattern. The theoretical results show the capabilities of the analytical derivation as well as the proposed technique in forming specific radiation patterns.

OCIS codes: 010.3640, 030.1670, 070.6110.

doi: 10.3788/COL201311.080102.

Phased array technology, originally developed in the 1 950s[1], has recently been used in a broad range of applications in satellite communications, weather radar, nondestructive detection, medical diagnosis, underground exploration, smart antenna, etc.[2−7]. The primary objective of this technique is to build far-field radiation patterns with high main lobe and low side lobes in a desired direction by the coherent radiation superposition of the array elements. To reinforce the radiation pattern, the relative phases of individual elements are precisely adjusted while their respective amplitudes are equal[8−14]. In general, the phased array encounters difficulty in forming any target radiation pattern, such as a ring or rectangular shape, despite the ring-shaped radiation pattern's applications in directed and wartime communications and specific shape ultrasonic therapy. In addition, delay lines applied in phased arrays become short especially at the optical wavelength and are difficult to fabricate, making phase shifters complicated and costly.

In describing radiation fields, amplitude is another important factor aside from the phase. In this study, the radiation pattern in the far field is theoretically investigated by manipulating the radiation amplitudes in an in-phase radiation array. As a result, a universal formula which determines the relationship between the radiation amplitudes of array elements and a random symmetrical radiation pattern in the far field is derived. This formula provides a novel discovery that any desired radiation pattern could be formed by simply controlling the respective radiation amplitude (i.e., amplitude weight) of array elements with these radiation amplitudes determined by solving the formula analytically. Distinct from phased array technology, this amplitude-weighting array technology only requires the utilization of variable attenuators in each radiation element and avoids the use of phase shifters.

Furthermore, to confirm the validity of this method, an annular radiation pattern is chosen as target far-field pattern, after which the radiation amplitude of each array element is determined by solving the formula analytically. The available far-field pattern is calculated by applying these solutions and comparing it with the target far-field pattern.

We will build the universal formula for amplitude-weighting array technology to describe the relationship between the radiation amplitudes of array elements and a symmetrical radiation pattern in the far field. Figure 1 illustrates a planar array with $(2N+1)\times(2M+1)$ elements in an isotropic media and Cartesian coordinate system. The elements of this array are distributed symmetrically in plane xoy with the axial spacing of a and b in the x-axis and y-axis directions, respectively. The coordinates of the far-field point P is $(x_0,\ y_0,\ z_0)$, $\overrightarrow{L}_0$ denotes the vector from origin o to point P, θ denotes the angle between z-axis and the projection of $\overrightarrow{L}_0$ in plane xoy, and ϕ denotes the angle between the z-axis and the projection of $\overrightarrow{L}_0$ in plane yoz. To simplify, all the array elements are regarded as ideal point radiation sources with identical circular frequency ω and polarization direction.

Starting with a random array element C with coordinates $(na,\ mb)$ $(-N \leqslant n \leqslant N,\ -M \leqslant m \leqslant M)$, a line

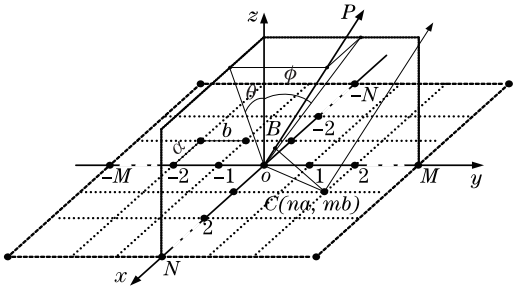

Fig. 1. Planar array elements distributed symmetricall in plane xoy.

that crosses $\overrightarrow{L}_0$ perpendicularly at point $B(x,\ y,\ z)$ is drawn. $\overline{OB}^2 = x^2 + y^2 + z^2$ is the wave path distance between element C and origin array element $O(0,\ 0)$ and can be written as

$$\overline{OB}^2 = x^2 + y^2 + z^2. \tag{1}$$

After simple calculations, we obtain

$$\overline{OC}^2 - \overline{BC}^2 = xna + ymb. \tag{2}$$

Using $\overline{OB}^2 = \overline{OC}^2 - \overline{BC}^2$, the following equation can be derived:

$$x^2 + y^2 + z^2 = xna + ymb. \tag{3}$$

Using the following equations,

$$x = z\tan\theta, \quad y = z\tan\phi,$$
$$z = \frac{na\tan\theta + mb\tan\phi}{1 + \tan^2\theta + \tan^2\phi}, \tag{4}$$

and the wave path distance $\overline{OB}$ can be rewritten as

$$\overline{OB} = \overline{OB}_{n,m}(\theta,\ \phi) = \frac{na\tan\theta + mb\tan\phi}{\sqrt{1 + \tan^2\theta + \tan^2\phi}}. \tag{5}$$

The vibration at point P caused by any element of $C(na,\ mb)$ is given by

$$p_{n,m}(\overrightarrow{L}_0, t) = A_{n,m}\cos\left[\omega t - kL_0 + k\overline{OB}_{n,\ m}\ (\theta,\ \phi)\right], \tag{6}$$

where k is wave number. Considering that the polarization directions of the radiation from all array elements are the same at the far-field point P, the total vibration at point P caused by this $(2N+1)\times(2M+1)$ array can be considered as the vibration summation of all individual elements and could therefore be expressed as

$$p(\overrightarrow{L}_0, t) = \sum_{n=-N}^{N}\sum_{m=-M}^{M} p_{n,m}(\overrightarrow{L}_0, t) = \sum_{n=-N}^{N}\sum_{m=-M}^{M} A_{n,m}\cos\left[\omega t - kL_0 + \frac{kna\tan\theta}{\sqrt{1 + \tan^2\theta + \tan^2\phi}} + \frac{kmb\tan\phi}{\sqrt{1 + \tan^2\theta + \tan^2\phi}}\right]. \tag{7}$$

In the present study, focus is given on the distribution of radiation amplitude in space. To separate the time variable from the space variable and obtain $A_{n,m}$ analytically from the above equation, a constraint is imposed on $A_{n,m}$ by assuming that $A_{n,m}$ is symmetrical. This implies that the radiation pattern in the far-field is symmetrical with the z-axis. Thus,

$$A_{n,\ m} = A_{n,\ -m} = A_{-n,\ m} = A_{-n,\ -m}, \tag{8}$$

and

$$p(\overrightarrow{L}_0, t) = \left[\sum_{n=-N}^{N}\sum_{m=-M}^{M} A_{n,m}\cos\left(\frac{nka\tan\theta}{\sqrt{1 + \tan^2\theta + \tan^2\phi}}\right)\cos\left(\frac{mkb\tan\phi}{\sqrt{1 + \tan^2\theta + \tan^2\phi}}\right)\right]\cos(\omega t - kL_0) = p(\theta,\phi)\cos(\omega t - kL_0). \tag{9}$$

Equation (9) indicates that the vibration at point P is in harmonic motion with angular frequency ω and amplitude $p(\theta,\ \phi)$ as denoted by

$$p(\theta,\phi) = \sum_{n=-N}^{N}\sum_{m=-M}^{M} A_{n,m}\cos\left(\frac{nka\tan\theta}{\sqrt{1 + \tan^2\theta + \tan^2\phi}}\right)\cos\left(\frac{mkb\tan\phi}{\sqrt{1 + \tan^2\theta + \tan^2\phi}}\right). \tag{10}$$

Equation (10) shows the far-field amplitude distribution of a radiation pattern. The maximum of $p(\theta,\ \phi)$ obviously occurs at θ=0 and ϕ=0. Furthermore, for the far-field point P, both θ and ϕ are assumed small. Therefore, the following approximation can be derived:

$$1 + \tan^2\theta + \tan^2\phi \approx 1 + \tan^2\theta \approx 1 + \tan^2\phi. \tag{11}$$

By using the far-field approximation of Eq. (11), Eq. (10) can be written as the function of separation of the variables θ and ϕ with the following form:

$$p(\theta,\phi) = \sum_{n=-N}^{N}\sum_{m=-M}^{M} A_{n,m}\cos(nka\sin\theta)\cos(mkb\sin\phi). \tag{12}$$

Herein, two parameters ξ and η with the following definitions can be introduced:

$$\xi = ka\sin\theta, \tag{13}$$

$$\eta = kb\sin\phi. \tag{14}$$

Substituting these parameters into Eq. (12) and considering the symmetry of $A_{n,m}$, Eq. (12) takes the following form

$$p(\xi,\eta) = \sum_{n=-N}^{N}\sum_{m=-M}^{M} A_{n,m}\cos(n\xi)\cos(m\eta) = \sum_{n=-N}^{N}\sum_{m=-M}^{M} A_{n,m}\mathrm{e}^{-\mathrm{j}(n\xi+m\eta)}, \tag{15}$$

where $A_{n,m}\mathrm{e}^{-\mathrm{j}(n\xi+m\eta)}$ can be reasonably taken as the contribution of element $(n,\ m)$ to the spatial radiation pattern $p(\xi,\eta)$. Array element spacing a, b and radiation wavelength λ are assumed to satisfy the following relationship:

$$a \geqslant \frac{\lambda}{2}, \quad b \geqslant \frac{\lambda}{2}. \tag{16}$$

The relationship observed in Eq. (16) can be called a half-constraint condition, which means that both ξ and η fall within the range of $[-\pi,\ \pi]$. Multiplying both sides of Eq. (15) by the factor $\frac{1}{4\pi^2}e^{j(n_0\xi+m_0\eta)}$ and then doubly integrating them by ξ and η, respectively, will result in

the following relation:

$$\begin{aligned}&\frac{1}{4\pi^2}\int_{\xi=-\pi}^{\pi}\int_{\eta=-\pi}^{\pi}p(\xi,\eta)\mathrm{e}^{\mathrm{j}(n_0\xi+m_0\eta)}\mathrm{d}\xi\mathrm{d}\eta\\&=\sum_{n=-N}^{N}\sum_{m=-M}^{M}A_{n,m}\frac{1}{4\pi^2},\\&\int_{\xi=-\pi}^{\pi}\mathrm{e}^{-\mathrm{j}(n-n_0)\xi}\mathrm{d}\xi\int_{\eta=-\pi}^{\pi}\mathrm{e}^{-\mathrm{j}(m-m_0)\eta}\mathrm{d}\eta\\&=\begin{cases}A_{n_0,m_0} & (n=n_0,m=m_0)\\0 & (n\neq n_0,m\neq m_0)\end{cases}.\end{aligned}\tag{17}$$

According to Eq. (17), the radiation amplitude $A_{n,m}$ of element (n, m) can be easily obtained by

$$\begin{aligned}A_{n,m}=&\frac{1}{4\pi^2}\int_{\xi=-\pi}^{\pi}\int_{\eta=-\pi}^{\pi}p(\xi,\eta)e^{j(n\xi+m\eta)}\mathrm{d}\xi\mathrm{d}\eta\\&\big(-N\leqslant n\leqslant N,-M\leqslant m\leqslant M\big).\end{aligned}\tag{18}$$

Equation (18) clearly depicts the mathematical relationship between the spatial radiation pattern $p(\xi, \eta)$ and the radiation amplitude $(A_{n,m})$ of any array element. This formula acts as the basis of the amplitude-weighted array technology and provides the novel discovery that any desired symmetrical radiation pattern could be formed by simply controlling the respective radiation amplitude (i.e., amplitude weight) of array elements with these radiation amplitudes solved by this formula. The formula is always valid under the half-constraint condition and far-field approximation. Furthermore, for the practical application of this technology, all the array elements maintains constant phase and only their amplitudes vary. Thus, this technology only requires the utilization of variable attenuators in each radiation element instead of utilizing a phase shifter.

Given that Eq. (18) shows the relationship between a symmetric beam pattern and a phase-invariant (i.e., amplitude-only-variant) weight pattern, this equation may be thought to be consistent with the formula given in Ref. [15]. However, Ref. [15] did not provide a rigorous discussion of the planar array and apertures in the following aspects. In Ref. [15], Van Trees multiplied the one-dimensional (1D) x-direction space distribution formula of radiation amplitude by the 1D y-direction space distribution formula of radiation amplitude. This product was extended to the radiation amplitude space distribution of a two-dimensional (2D) planar array, as shown in Eq. (4.25) of Ref. [15]. However, this is not entirely true. Instead, we established a radiation amplitude distribution formula of a planar array in Eq. (7) directly in three-dimensional (3D) space. To obtain an analytical expression for the radiation amplitude of an array element, a small-angle approximation was applied to Eq. (10). Thus, the two space variables were separated from each other and Eq. (18) was obtained, which is consistent with Van Trees' work. In the current work, Eq. (18) is merely an approximate expression that is only used to compute the radiation amplitude of array element $A_{n,m}$. Finally, $A_{n,m}$ would be substituted into the original formula of radiation pattern in Eq. (10). The space variables θ and ϕ notably exist in two multiplied functions of Eq. (10) although they are separated in Eq. (4.25) of Ref. [15], which largely differentiates the present study with Van Trees' work.

Next, the validity of Eq. (18) is confirmed through the so-called amplitude-weighted array technology. To simplify the calculation, the desired radiation pattern is assumed annular with a constant intensity. Let Ω_1 and Ω_2 be two solid angles corresponding to the inner and outer boundaries of this pattern, respectively. The generalized intensity or amplitude of the annular radiation pattern can then be described as

$$p_1(\theta,\phi)=\begin{cases}1 & (\Omega_1^2\leqslant\theta^2+\phi^2\leqslant\Omega_2^2)\\0 & (\theta^2+\phi^2\geqslant\Omega_2^2 \text{ or } \theta^2+\phi^2\geqslant\Omega_1^2)\end{cases}.\tag{19}$$

Furthermore, to simplify the calculation, the axial spacing of array elements is assumed to satisfy the following relationship:

$$a=b=\frac{\lambda}{2}.\tag{20}$$

By substituting Eq. (20) into Eq. (13), the following formulas are obtained:

$$\begin{cases}\xi=\pi\sin\theta & (-\pi\leqslant\xi\leqslant\pi)\\\eta=\pi\sin\phi & (-\pi\leqslant\eta\leqslant\pi)\end{cases}.\tag{21}$$

Thereafter, by substituting Eqs. (19) and (21) into Eq. (18), the radiation amplitude unit $A_{n,m}$ can be given by

$$\begin{aligned}A_{n,m}=&\frac{1}{4}\int_{\theta=-\frac{\pi}{2}}^{\frac{\pi}{2}}\int_{\phi=-\frac{\pi}{2}}^{\frac{\pi}{2}}p_1(\theta,\phi)\mathrm{e}^{\mathrm{j}(n\pi\sin\theta+m\pi\sin\phi)}\\&\cos\theta\cos\phi\mathrm{d}\theta\mathrm{d}\phi\\=&\int_{\theta=0}^{\Omega_1}\int_{\phi=\sqrt{\Omega_1^2-\theta^2}}^{\sqrt{\Omega_2^2-\theta^2}}\cos(n\pi\sin\theta)\cos(m\pi\sin\phi)\cos\theta\cos\phi\mathrm{d}\theta\mathrm{d}\phi\\&+\int_{\theta=\Omega_1}^{\Omega_2}\int_{\phi=0}^{\sqrt{\Omega_2^2-\theta^2}}\cos(n\pi\sin\theta)\cos(m\pi\sin\phi)\cos\theta\cos\phi\mathrm{d}\theta\mathrm{d}\phi\\=&\int_{\phi=0}^{\Omega_1}\int_{\theta=\sqrt{\Omega_1^2-\phi^2}}^{\sqrt{\Omega_2^2-\phi^2}}\cos(n\pi\sin\theta)\cos(m\pi\sin\phi)\cos\theta\cos\phi\mathrm{d}\theta\mathrm{d}\phi\\&+\int_{\phi=\Omega_1}^{\Omega_2}\int_{\theta=0}^{\sqrt{\Omega_2^2-\phi^2}}\cos(n\pi\sin\theta)\cos(m\pi\sin\phi)\cos\theta\cos\phi\mathrm{d}\theta\mathrm{d}\phi,\end{aligned}\tag{22}$$

where $-N\leqslant n\leqslant N$ and $-M\leqslant m\leqslant M$. After further calculations, $A_{n,m}$ can be written as

$$A_{n,m}=\begin{cases}\int_0^{\Omega_2}\cos\theta\sin\sqrt{\Omega_2^2-\theta^2}\mathrm{d}\theta-\int_0^{\Omega_1}\cos\theta\sin\sqrt{\Omega_1^2-\theta^2}\mathrm{d}\theta & (n=m=0)\\ \int_0^{\Omega_2}\cos(m\pi\sin\phi)\cos\phi\sin(\sqrt{\Omega_2^2-\phi^2})\mathrm{d}\phi-\int_0^{\Omega_1}\cos(m\pi\sin\phi)\cos\phi\sin(\sqrt{\Omega_1^2-\phi^2})\mathrm{d}\phi & (n=0,\ m\neq 0)\\ \int_0^{\Omega_2}\cos(n\pi\sin\theta)\cos\theta\sin(\sqrt{\Omega_2^2-\theta^2})\mathrm{d}\theta-\int_0^{\Omega_1}\cos(n\pi\sin\theta)\cos\theta\sin(\sqrt{\Omega_1^2-\theta^2})\mathrm{d}\theta & (n\neq 0,\ m=0)\\ \frac{1}{n\pi}\int_0^{\Omega_2}\cos\phi\cos(m\pi\sin\phi)\sin(n\pi\sin\sqrt{\Omega_2^2-\phi^2})\mathrm{d}\phi-\frac{1}{n\pi}\int_0^{\Omega_1}\cos\phi\cos(m\pi\sin\phi)\sin(n\pi\sin\sqrt{\Omega_1^2-\phi^2})\mathrm{d}\phi & (n\neq 0,\ m\neq 0)\end{cases}. \tag{23}$$

The expression in Eq. (23) evaluates any radiation amplitude unit $A_{n,m}$ in forming an annular radiation pattern in the far field. The following relationships can be easily deduced from Eq. (23):

$$\begin{cases}A_{n,0}=A_{0,m} & (n=m)\\ A_{n,m}=A_{n,-m}=A_{-n,m}=A_{-n,-m} & (n\neq 0, m\neq 0)\end{cases}. \tag{24}$$

Equation (24) shows the symmetry of radiation amplitudes of array elements relative to the origin and axes of the coordinate system, and this symmetry originates from the symmetrical intensity distributions of the desired far-field radiation pattern relative to the z axis.

Furthermore, by substituting Eqs. (23) and (24) into Eq. (10), the amplitude $p(\theta,\ \phi)$ of the available far-field radiation pattern could be given by

$$p(\theta,\ \phi)=A_{0,0}+2\sum_{n=1}^{N}A_{n,0}\cos(n\Theta)+2\sum_{m=1}^{M}A_{0,m}\cos(m\Phi)+4\sum_{n=1}^{N}\sum_{m=1}^{M}A_{n,m}\cos(n\Theta)\cos(m\Phi), \tag{25}$$

where

$$\Theta=\frac{ka\tan\theta}{\sqrt{1+\tan^2\theta+\tan^2\phi}}=\frac{\pi\tan\theta}{\sqrt{1+\tan^2\theta+\tan^2\phi}},$$
$$\Phi=\frac{kb\tan\phi}{\sqrt{1+\tan^2\theta+\tan^2\phi}}=\frac{\pi\tan\phi}{\sqrt{1+\tan^2\theta+\tan^2\phi}}. \tag{26}$$

This relation implies that if the radiation amplitudes of the array elements $A_{n,\,m}$ take the values shown in Eq. (23), the actual radiation amplitude distribution in the far-field, $p(\theta,\ \phi)$, provided by the planar array must be Eq. (25). In fact, the target far-field radiation amplitude $p_1(\theta,\ \phi)$ defined in Eq. (19) is a step function. Therefore, the manner by which $p(\theta,\ \phi)$ approaches $p_1(\theta,\ \phi)$ reflects the effectiveness of the universal formula of Eq. (18) in amplitude-weighted array technology.

As a result, Figs. 2 and 3 plot the available far-field radiation amplitude $p(\theta,\ \phi)$ under different array elements at $\Omega_1=\pi/18$ (in radians) and $\Omega_2=\pi/20$ (in radians). As seen in these plots, the available far-field radiation amplitude exhibits a nearly doughnut-shaped intensity distribution studded with several local intensity spikes along the annular profiles when the numbers of array elements are small. Nevertheless, when the numbers of array elements increase, the uniformity of the spatial radiation pattern $p(\theta,\ \phi)$ is significantly improved, while the local intensity spikes along its annular profile disappear.

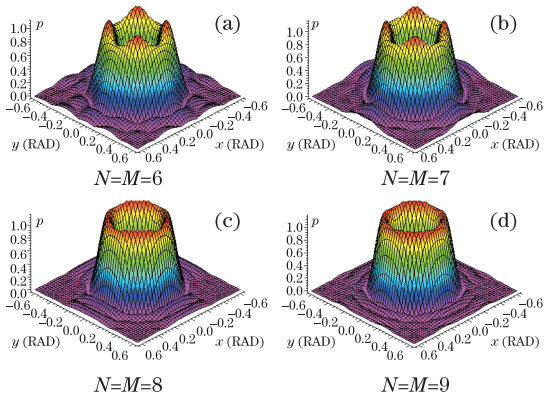

Fig. 2. (Color online) 3D view of available far-field radiation patterns.

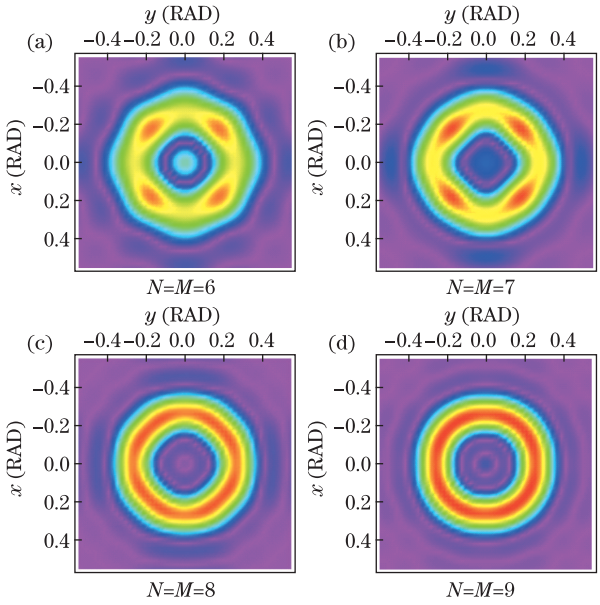

Fig. 3. (Color online) Top view of available far-field radiation pattern at different array elements.

Table 1. Energy Ratios under Different Numbers of Array Elements

Number of Array Elements $(2N+1)\times(2M+1)$	Energy Ratio (%) R
13×13	63.17
15×15	70.05
17×17	81.89
19×19	92.13
35×35	95.17
49×49	97.0

Figure 4 plots the corresponding line profiles of stimulated far-field radiation patterns at x=0 under different array elements, and each is compared with the rectangular line profiles of the target far-field radiation pattern. With the increase of array elements, the radiation pattern $p(\theta, \phi)$ is gradually concentrated within the identical solid angle range with that of the target radiation pattern $p_1(\theta, \phi)$.

To quantitatively evaluate the extent by which the available far-field radiation amplitude $p(\theta, \phi)$ approaches the target function $p_1(\theta, \phi)$, an energy ratio must be defined:

$$R=\frac{E_{\text{main}}}{E_{\text{total}}}=\int_{\theta=0}^{\Omega_1}\int_{\phi=\sqrt{\Omega_1^2-\theta^2}}^{\sqrt{\Omega_2^2-\theta^2}}|p(\theta,\phi)|^2\,\mathrm{d}\theta\mathrm{d}\phi+\int_{\theta=\Omega_1}^{\Omega_2}\int_{\phi=0}^{\sqrt{\Omega_2^2-\theta^2}}|p(\theta,\phi)|^2\,\mathrm{d}\theta\mathrm{d}\phi/\int_{\theta=0}^{\pi/2}\int_{\phi=0}^{\pi/2}|p(\theta,\phi)|^2\,\mathrm{d}\theta\mathrm{d}\phi, \quad (27)$$

where the numerator E_{main} denotes the radiation energy of the practical radiation pattern distributed in the identical solid angle with that of the target radiation pattern, while the denominator E_{total} denotes the total radiation energy of the practical radiation pattern. The calculated energy ratios R under different array element numbers are listed in Table 1. R increases with increasing array element numbers, and if an energy ratio larger than 90% is required, the array elements should be equal to or larger than 361, i.e., $N = M \geqslant 9$.

As discussed above, any desired and symmetrical radiation pattern can be formed based on the amplitude-weighted method. Nevertheless, to obtain an analytical expression for the radiation amplitude of an array element, small-angle approximations were applied to Eq. (10) such that the variables θ and ϕ could be separated in Eq. (12), thereby resulting in more analytical expressions. To estimate the error between the formed radiation pattern and the desired radiation pattern caused by this approximation, the item of series in Eq. (10) is taken and represented by

$$S_{nm}(\theta,\phi)=\cos\Big(\frac{nka\tan\theta}{\sqrt{1+\tan^2\theta+\tan^2\phi}}\Big)\cos\Big(\frac{mkb\tan\phi}{\sqrt{1+\tan^2\theta+\tan^2\phi}}\Big). \quad (28)$$

After applying the small-angle approximation as shown in Eq. (10), Eq. (28) can be rewritten as

$$\widetilde{S}_{nm}(\theta,\phi)\approx\cos\Big(\frac{nka\tan\theta}{\sqrt{1+\tan^2\theta}}\Big)\cos\Big(\frac{mkb\tan\phi}{\sqrt{1+\tan^2\phi}}\Big). \quad (29)$$

Therefore, the approximation operation above will introduce an error (or difference) factor of $E(\theta, \phi)$ in the far-field radiation pattern $p(\theta, \phi)$ with the following form:

$$E(\theta,\phi)=\sum_{n=-N}^{N}\sum_{m=-M}^{M}A_{n,m}\Big[S_{nm}(\theta,\phi)-\widetilde{S}_{nm}(\theta,\phi)\Big]. \quad (30)$$

Using Eq. (30), $E(\theta, \phi)$ is zero when $\theta = 0$ or $\phi = 0$, which means that the small-angle approximation has no influence on radiation pattern as long as the radiation directions lie in the yoz plane or the xoz plane. Moreover, the value of error $E(\theta, \phi)$ not being equal to zero when $\theta = \phi \neq 0$ indicates that the actual radiation distribution will vary if the radiation directions lie in the two planes that bisect the yoz plane or the xoz plane (the two diagonals in Fig. 3), namely,

$$E(0,\phi)=\sum_{n=-N}^{N}\sum_{m=-M}^{M}A_{n,m}\big[S_{nm}(0,\phi)-\widetilde{S}_{nm}(0,\phi)\big]=0, \quad (31)$$

$$E(\theta,0)=\sum_{n=-N}^{N}\sum_{m=-M}^{M}A_{n,m}\big[S_{nm}(\theta,0)-\widetilde{S}_{nm}(\theta,0)\big]=0, \quad (32)$$

$$E(\theta,\phi)\,|_{\theta=\phi}=\sum_{n=-N}^{N}\sum_{m=-M}^{M}A_{n,m}\Big[\cos\Big(\frac{nka\tan\theta}{\sqrt{1+2\tan^2\theta}}\Big)\cos\Big(\frac{mkb\tan\theta}{\sqrt{1+2\tan^2\theta}}\Big)-\cos\Big(\frac{nka\tan\theta}{\sqrt{1+\tan^2\theta}}\Big)\cos\Big(\frac{mkb\tan\theta}{\sqrt{1+\tan^2\theta}}\Big)\Big]. \quad (33)$$

Herein, the sample above is still considered and the error in Eq. (33) is calculated quantitatively. Figure. 5 plots the calculated error $E(\theta)$ as a function of θ under different array elements of $N = M$. The error $E(\theta)$ oscillates with θ and a maximum $E(\theta_0)$ exists at a certain angle θ_0. This maximum error $E(\theta_0)$, the desired radiation amplitude $p(\theta_0,\theta_0)$ and its approximation $\widetilde{p}(\theta_0, \theta_0)$, the relative error $E(\theta_0)/p(\theta_0, \theta_0)$, and the maximum of radiation amplitude $p_{\max}(\theta, \phi)$ are summarized in Table 2.

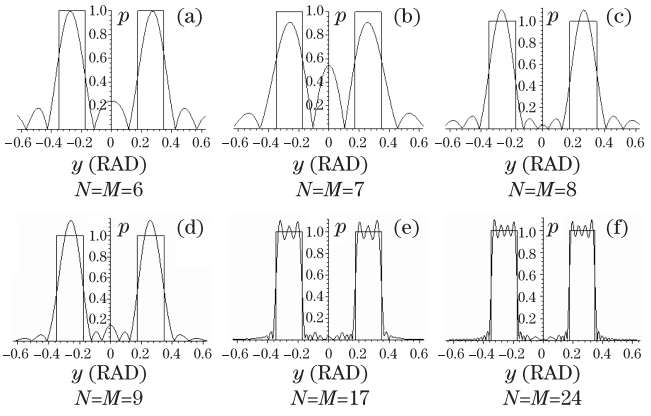

Fig. 4. Comparison of the line profiles of available far-field radiation patterns for different array elements at x=0 with the rectangular line profiles of the target far-field radiation pattern.

Table 2. Calculated Radiation Parameters under Different Numbers of Array Elements

Number of Array Elements $(2N+1)\times(2M+1)$	θ_0(deg.)	$p(\theta_0,\ \theta_0\ )$	$\widetilde{p}(\theta_0,\theta_0)$	Absolute Error $E(\theta_0\ )$	Relative Error $E(\theta_0\ )/p(\theta_0,\theta_0)$	$p_{\max}(\theta,\ \phi)$ $(=p(0,0))$
13×13	26.1672	2.447852	0.406883	2.040969	83.3779	169.0
15×15	31.9781	2.220776	0.014173	2.206604	99.3618	225.0
17×17	27.4942	2.568723	0.126813	2.441910	95.0632	289.0
19×19	24.1672	2.881674	0.322951	2.558723	88.7929	361.0
35×35	19.7030	3.971881	0.373965	3.597916	90.6020	1225.0
49×49	18.9076	4.49050	0.152512	4.337988	96.6037	2401.0

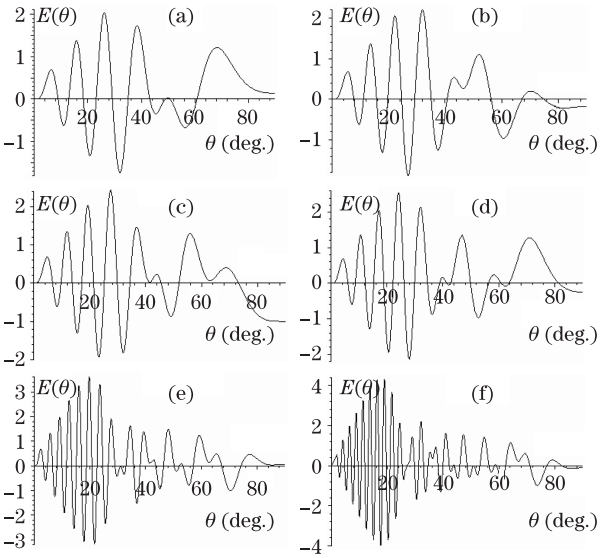

Fig. 5. Graphs of absolute error $E(\theta)$ under different array elements of (a) 13×13, (b) 15×15, (c) 17×17, (d) 19×19, (e) 35×35, and (f) 49×49 by using $A_{n,m}\equiv 1$, $ka{=}kb{=}\pi$.

The maximum error $E(\theta_0)$ increases with increasing number of array elements. However, the angle θ_0 at which the maximum of the error $E(\theta)$ occurs would decrease with increasing number of array elements. At a specific number of array elements, the error $E(\theta)$ is bound in the effective range of radiation angles (θ and ϕ), which is also much less than the maximum of radiation amplitude $p_{\max}(\theta,\ \phi)$ at a large radiation angle. Therefore, beam-forming not only with small radiation angles but also with larger radiation angles can be implemented by means of the amplitude-weighting method. In other words, the small angle approximation has little influence on beam forming.

In conclusion, an analytical formula describing the relationship between the radiation amplitudes of planar array elements and a symmetrical far-field radiation pattern in an amplitude-weighted array system under the half-constraint condition and far-field approximation is derived. Using this formula, any desired symmetrical far-field radiation pattern with smaller radiation solid angles could be formed by simply controlling the respective radiation amplitude (i.e., amplitude weight) of the array elements with these radiation amplitudes determined analytically. In addition, the quality of the far-field radiation pattern formed by using the solved radiation amplitudes (i.e., amplitude weights) of all array elements can be estimated by the energy ratio R. The simplicity of amplitude-weighted array technology in using this analytical formula provides potential applications in special communications, medical diagnosis and treatment, and well logging.

This work was supported by the Shaanxi Province Natural Science Foundation of China under Grant No. SJ08ZT04-6.

References

1. W. H. Von Aulock, in *Proceedings of the IRE 48* 1715 (1960).
2. K. Sato, K. Nishikawa, and T. Hirako, in *Proceedings of Antennas and Propagation Society International Symposium 2* 1073 (1992).
3. D. E. Forsyth, J. F. Kimpel, D. S. Zrnic, S. Sandgathe, C. F. Pfeil, J. F. Heimmer, T. McNellis, J. E. Crain, A. M. Shapiro, J. D. Belville, and W. Benner, in *Proceedings of 32nd Conference on Radar Meteorology* 24 (2008).
4. A. N. Guz' and F. G. Makhort, Int. Appl. Mech. **36,** 1119 (2000).
5. M. O'Donnell, M. J. Eberle, D. N. Stephens, J. L. Litzza, K. S. Vicente, and B. M. Shapo, in *Proceedings of Ultrasonics Symposium, IEEE 2* 1251 (1995).
6. M. L. Wolfson, D. F. Naar, P. A. Howd, S. D. Locker, B. T. Donahue, C. T. Friedrichs, A. C. Trembanis, M. D. Richardson, and T. F. Wever, IEEE J. Ocean. Eng. **32,** 103 (2007).
7. A. Alexiou and M. Haardt, IEEE Commun. Mag. **42,** 90 (2004).
8. M. G. Bray, D. H. Werner, D. W. Boeringer, and D. W. Machuga, IEEE Trans Antenn. Propag. **50,** 1732 (2002).
9. D. W. Boeringer, D. H. Werner, and D. W. Machuga, IEEE Trans Antenn. Propag. **53,** 356 (2005).
10. C. Rocha-Alicano, D. Covarrubias-Rosales, C. Brizuela-Rodriguez, and M. Panduro-Mendoza, AEU-International Journal of Electronics and Communications **61,** 286 (2007).
11. T. Yuan, N. Yuan, J. L.-W. Li, and M. -S. Leong, Progress In Electromagnetics Research **87,** 131 (2008).
12. K. Nishimura and T. Sato, IEICE Trans. Commun. **E92-B,** 3228 (2009).
13. N. I. Dib, S. K. Goudos, and H. Muhsen, Progress in Electromagnetics Research **102,** 159 (2010).
14. K. A. Papadopoulos, C. A. Papagianni, P. K. Gkonis, I. S. Venieris, and D. I. Kaklamani, Progress in Electromagnetics Research M **17,** 237 (2011).
15. H. L. Van Trees, *Optimum Array Processing, Part IV of Detection, Estimation, and Modulation Theory* (John Wiley & Sons, Inc., New York, 2002).